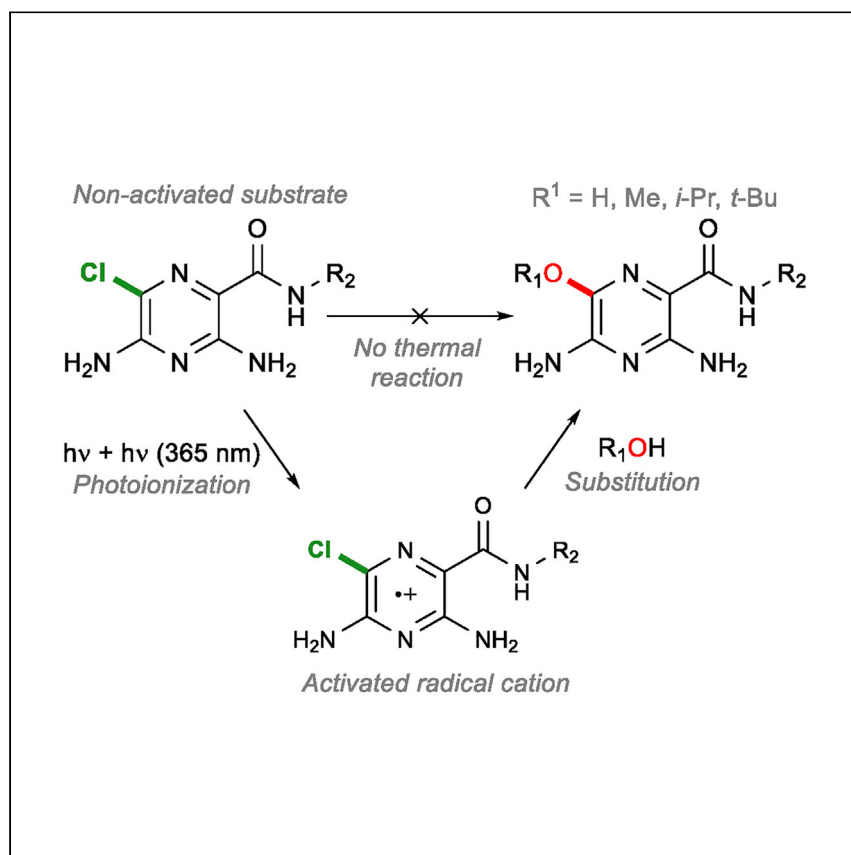


Article

Degradation of Pharmaceuticals through Sequential Photon Absorption and Photoionization in Amiloride Derivatives



Kjell Jorner, Wangchuk Rabten, Tomas Slanina, ..., Jufang Wu Ludvigsson, Henrik Ottosson, Per-Ola Norrby

henrik.ottosson@kemi.uu.se (H.O.)
per-ola.norrby@astrazeneca.com (P.-O.N.)

HIGHLIGHTS

Amiloride derivatives undergo photosubstitution in protic solvents

Mechanism goes via photoionization by sequential absorption of two photons

Photoionization may be triggered by antiaromaticity of the excited state

The mechanism has parallels with methods in synthetic photoredox chemistry

Haloaromatic drug molecules of the amiloride family are plagued by photodegradation with associated toxicity. Jorner et al. show photodegradation via substitution in water and other protic solvents. The mechanism likely goes via photoionization by sequential absorption of two photons and has striking parallels with recent methods in synthetic photoredox chemistry.

Article

Degradation of Pharmaceuticals through Sequential Photon Absorption and Photoionization in Amiloride Derivatives

Kjell Jorner,^{1,2} Wangchuk Rabten,¹ Tomas Slanina,^{1,3} Nathalie Proos Vedin,¹ Sara Sillén,⁴ Jufang Wu Ludvigsson,⁴ Henrik Ottosson,^{1,*} and Per-Ola Norrby^{5,6,*}

SUMMARY

Haloaromatic drug molecules of the amiloride family are plagued by photodegradation with associated toxicity. Herein, we report on the photodegradation of analogs of amiloride, which are known to undergo photosubstitution in water. Model compounds built on the same scaffold undergo clean photosubstitution also in alcoholic solvent, where a certain amount of photodehalogenation is normally expected. Available evidence points to a mechanism starting with photoexcitation followed by photoionization to give a radical cation intermediate. Subsequent substitution reaction with the protic solvent is assisted by a general base, possibly strengthened by the proximal solvated electron. Recombination with the solvated electron generates the observed product. Quantum chemical computations reveal that excited state antiaromaticity is relieved when an electron is ejected from the photoexcited molecule by the second photon. The mechanism indicated here could have wide applicability to photoinduced degradation of similar heteroaromatic compounds in the environment, as well as to a class of increasingly popular synthetic photoredox methods.

INTRODUCTION

Pharmaceutical research is aimed at increasing quality of life globally by finding cures to debilitating or fatal diseases. The progress in recent years has been astounding, but the route to a new drug still faces many obstacles, in particular regarding safety, that impede and increase the cost of pharmaceutical development. One important safety factor is drug product degradation, which can give impurities with potentially dangerous properties. The identification and investigation of all possible degradation products forms a significant part of the work that must precede the first dosing to human subjects. In some cases, degradation pathways are well understood and can be predicted using computational tools.¹ However, photochemical processes, leading to degradation and phototoxicity, are still less well understood than, for example, oxidative processes. Increased understanding of these processes could lead to better predictions of benefit to all drug development. The same processes are also important contributors to degradation of other substances in the environment, such as agrochemicals.

One of the most important photochemical degradation pathways of relevance to many drugs is photodehalogenation, which can occur either by photosubstitution, typically by the solvent, or photoreduction (Figure 1A).² For example, chlorpromazine, an antipsychotic drug, reacts by photosubstitution in water,^{3,4} although

¹Department of Chemistry – Ångström Laboratory, Uppsala University, Box 523, SE-75120 Uppsala, Sweden

²Early Chemical Development, Pharmaceutical Sciences, R&D, AstraZeneca, GB-SK102NA, Macclesfield, UK

³Institute of Organic Chemistry and Biochemistry of the Czech Academy of Sciences, Flemingovo nám. 2, 16610 Prague, Czech Republic

⁴Manufacturing Science & Technology, Pharmaceutical Technology & Development, AstraZeneca Gothenburg, SE-43183 Mölndal, Sweden

⁵Data Science and Modelling, Pharmaceutical Sciences, R&D, AstraZeneca Gothenburg, Pepparedsleden 1, SE-43183 Mölndal, Sweden

⁶Lead Contact

*Correspondence: henrik.ottosson@kemi.uu.se (H.O.), per-ola.norrby@astrazeneca.com (P.-O.N.)
<https://doi.org/10.1016/j.xcrp.2020.100274>



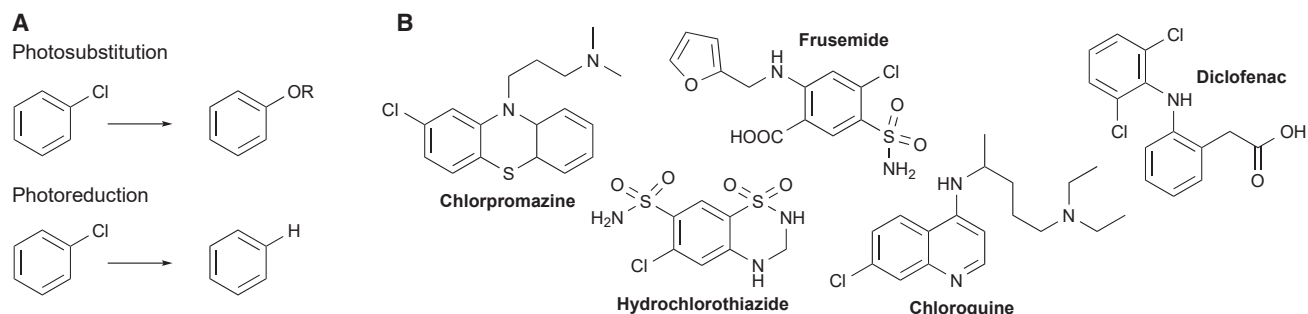


Figure 1. Photodegradation Pathways of Haloaromatic Drug Molecules

(A) Photosubstitution and photoreduction mechanism for dehalogenation of aromatic substrates.

(B) Examples of drug molecules undergoing photodehalogenation.

irradiation in methanol leads to both photoreduction and photosubstitution in a 1:1 ratio (Figure 1B). Reaction in more substituted alcohols favors the reduction product.⁵ As with most photodegradations, the complete product profile is complicated and highly dependent on the reaction conditions, e.g., presence of oxygen. Irradiation under conditions simulating the aquatic environment leads to a total of 57 photoproducts, the major ones from photosubstitution and oxidation.³ Another prominent drug undergoing photodehalogenation is diclofenac (Figure 1B). Upon irradiation, it undergoes ring closure and loss of one of the chlorine substituents to form a carbazole. Further irradiation leads to both photoreduction (major) and photosubstitution (minor) in water or methanol.⁶ Other drugs that undergo photo-dechlorination include frusemide,⁷ chloroquine,⁸ and hydrochlorothiazide (Figure 1B).⁹ In addition, similar photodegradations could occur in compounds used in the agrochemical sector.

The primary photoreaction of the diuretic drug amiloride (1) in water is substitution of Cl to give the hydroxylated product 1-OH (Figure 2).^{2,10} This substitution reactivity contrasts with similar compounds, e.g., frusemide and hydrochlorothiazide, which undergo both photosubstitution and photoreduction. One explanation put forth in the literature is that frusemide and hydrochlorothiazide form an ion-pair complex $[Ar-Cl]^{\bullet+} + [Ar-Cl]^{\bullet-}$ by electron transfer from one molecule in the excited state to another molecule in the ground state.¹⁰ The resulting $[Ar-Cl]^{\bullet+}$ radical cation reacts with solvent to form Ar-OH, while the $[Ar-Cl]^{\bullet-}$ radical anion cleaves off a chloride anion and abstracts a hydrogen atom from the solvent to form Ar-H. As 1 only gives the Ar-OH product, Moore and co-workers argued that the mechanism is different and suggested that substitution occurs by attack of the water solvent on the radical cation of 1, formed by photoionization.¹¹ The hypothesis was supported by the observation of photoionization of 1 in aqueous solution accompanied by the formation of solvated electrons at both 265 nm and 353 nm, as shown by Hamoudi et al.¹² The quantum yield of photoionization is 0.011 at pH 7 and increases with pH. The pH dependence of photoionization is similar to that of the quantum yield of amiloride photodegradation, which increases from 0.009 at low pH (4.0) to 0.023 at high pH (10.4), with an inflection point at \sim pH 8.¹¹ The location of the inflection point compares well with the pK_a of 1 at 8.7. It is expected that the neutral base form of amiloride would give away an electron more readily than the protonated, cationic form. Interestingly, Hamoudi did not observe the formation of solvated electrons in *i*-PrOH.¹² Instead, the triplet amiloride was postulated to abstract hydrogen from *i*-PrOH.

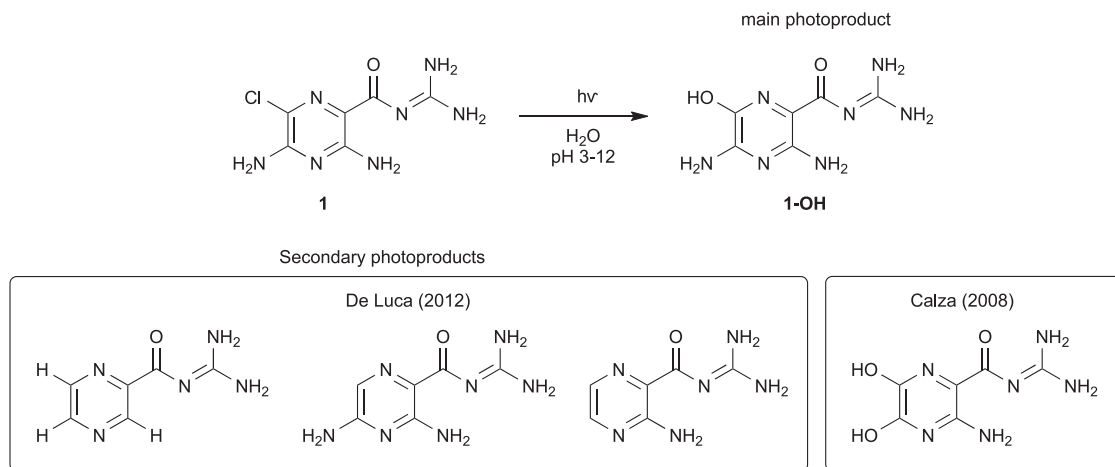


Figure 2. Photochemistry of Amiloride

Main (top) and secondary (bottom) photoproducts for amiloride (1) in H₂O.

Although the primary photoreaction of 1 is photosubstitution, the compound degrades further upon continued irradiation as its photoproduct 1-OH absorbs in the same region. Moore studied photodegradation under oxygen-free conditions using a medium pressure mercury lamp (Pyrex glass filter, >300 nm) and found that 1-OH forms with apparent first-order kinetics over the studied pH range of 4–11.¹⁰ The 1-OH product exists predominately as its keto tautomer. After ~50% conversion, unidentified secondary photoproducts started to appear. Using similar conditions, Calza and co-workers suggested a dihydroxy-substituted product that degraded upon continued irradiation (Figure 2).¹³ De Luca and co-workers studied the pH dependence at 300–800 nm under aerobic conditions and suggested three secondary photoproducts based on liquid chromatography (LC)-mass spectrometry (MS) analysis (Figure 2).¹⁴ An explanation for the discrepancy between these studies may be that Calza and co-workers used anaerobic conditions, promoting reactivity from the triplet state of 1 and preventing singlet oxygen-induced degradation pathways.

The photochemistry of 1 is dominated by the pyrazine moiety, and irradiation in water leads primarily to photosubstitution of the chlorine substituent.² The main pyrazine core in amiloride is central to its function and is found in many derivatives, such as benzamil, phenamil, DMA, EIPA, and HMA.¹⁵ To better understand the photodegradation mechanism of this family of compounds, we here investigate the amiloride analog 2 in water and other protic solvents (Figure 3A). We find that the primary photoreaction of 2 is photosubstitution by the solvent. The mechanism likely involves photoionization to the radical cation, induced by sequential absorption of two photons, followed by a concerted S_NAr-type reaction in which the chlorine is displaced by attack of solvent. This finding has implications not only for drug development but also synthetic organic chemistry. In recent years, photochemistry has emerged as a new way to access thermodynamically unfeasible modes of reactivity, opening previously inaccessible routes to target compounds.¹⁶ Of particular interest in this context is the work on substitution reactions of photochemically generated radical anions¹⁷ and cations. Pioneered by Pandey using 1,4-dicyanonaphthalene,¹⁸ this field has seen seminal contributions by, e.g., the groups of Fukuzumi,¹⁹ König,²⁰ Tung,²¹ and Nicewicz,²² who showed that photoredox chemistry could be harnessed to effect nucleophilic aromatic substitution (S_NAr) of nonactivated substrates. The

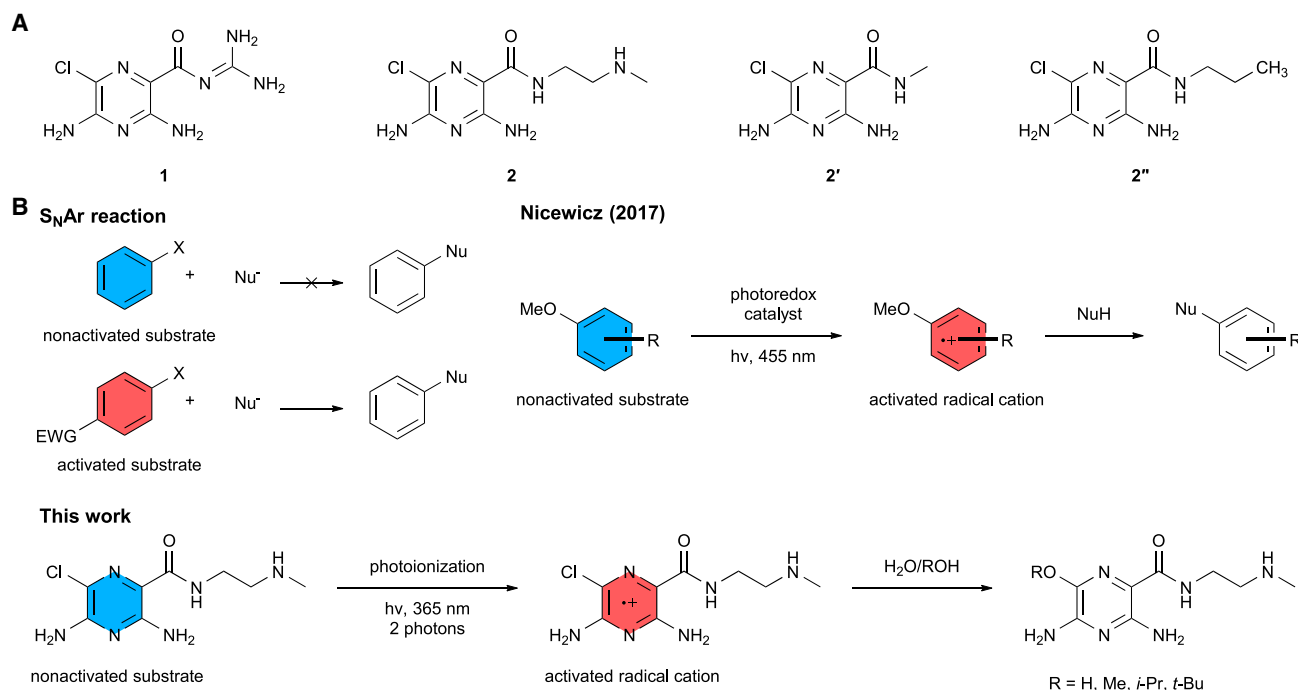


Figure 3. Amiloride Derivatives and Photochemistry through Nucleophilic Aromatic Substitution

(A) 1, experimentally studied derivative (2), computational model (2'), and derivative lacking terminal amino group (2'').

(B) S_NAr reactions generally require an activated substrate with electron-withdrawing groups. Oxidation by a photoredox catalyst can activate the substrate. Here, we show that photoionization by sequential absorption of two photons can also activate the substrate, without the need for a separate photoredox catalyst.

S_NAr reaction typically requires activated substrates carrying electron-withdrawing groups (Figure 3B), but photooxidation of the substrate to the radical cation can increase its reactivity substantially. Here, we show that similar reactivity can also be accessed without the use of a separate photoredox catalyst by sequential photoabsorption of the substrate to access the radical cation intermediate. This sequential photoabsorption is especially notable in light of recent work of Wenger²³ and König^{24,25} on harnessing the energy of two sequential photoexcitations to perform unprecedented transformations.

RESULTS AND DISCUSSION

Synthesis and Preliminary Experiments

To clarify the mechanism of the primary photoreactivity of the amiloride family, we chose to study compound 2 in detail. Compound 2 was synthesized in a single step from commercially available building blocks according to a literature procedure (Figure 4A).²⁶ The absorption spectrum in methanol shows three main peaks in the UV region, at 210 nm, 273 nm, and 360 nm (Figure 4). The spectrum of 2 is very similar to the spectrum of 1 in water, which has main peaks at 212 nm, 285 nm, and 362 nm.²⁷ TD-DFT calculations of 2 show that the photochemically relevant peaks at 360 nm (highest occupied molecular orbital [HOMO] \rightarrow lowest unoccupied molecular orbital [LUMO]) and at 273 nm (HOMO-2 \rightarrow LUMO+2) are of $\pi\pi^*$ character (see Supplemental Information, Table S3, and Figure S10).

Initial photochemical experiments at 350 nm in argon-saturated H_2O gave the hydroxy-substituted product 2-OH, showing that 2 reacts by photosubstitution in the same way as 1 (Table 1). Unfortunately, we were not able to determine the

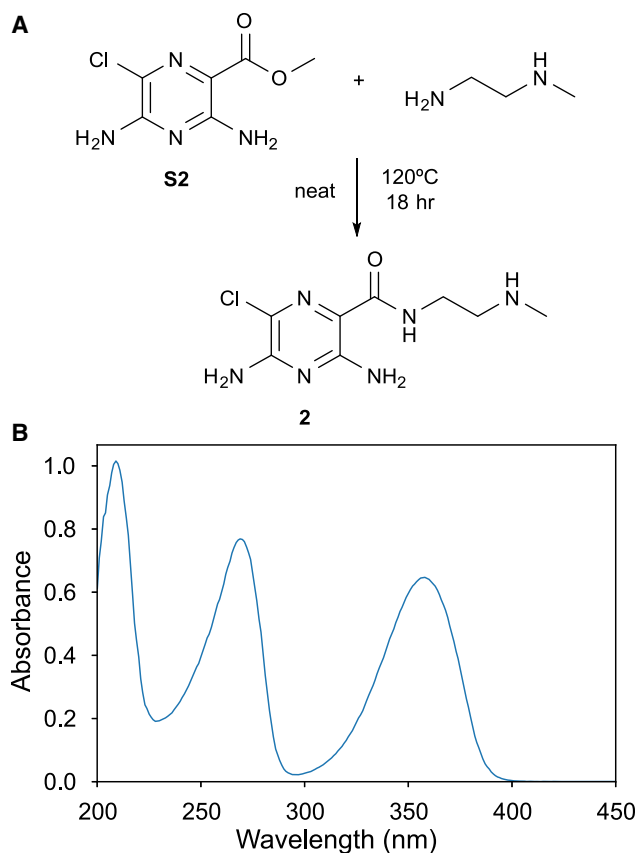


Figure 4. Compound 2

(A) Synthesis of 2.

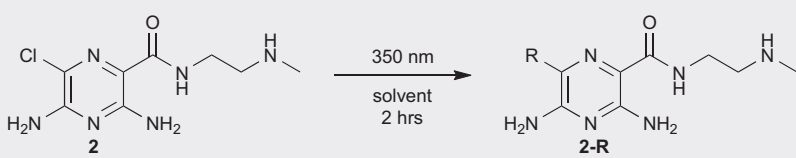
(B) Absorption spectrum of 2 in methanol.

nuclear magnetic resonance (NMR) yield due to the overlap between the reactant and the product peaks. In methanol, the methoxy-substituted 2-OMe was obtained with 68% NMR yield after 2 h of irradiation with traces of an unknown byproduct. Irradiation in the more substituted alcohol solvents EtOH, *i*-PrOH, and *t*-BuOH for the same time also resulted in photoreactivity but with lower NMR yields (60%, 46%, and 20%, respectively; entry 3–5). As far as we know, this is the first report of photoreactivity in alcoholic solvents for amiloride-like compounds. To test for the influence of the terminal amino group, we synthesized derivate 2'' (Figure 3), where the alkyl amine is replaced with a methyl group. Irradiation of 2'' under the standard conditions led to 57% NMR yield of the methoxy-substituted product 2''-OMe, showing that the terminal alkyl amine is not essential for the observed photoreactivity. Varying the light intensity using 2–16 of the lamps in the Rayonet reactor showed consistent reactivity with 2-OMe as the photoproduct (Figure S29).

Mechanistic Scenarios

In order to elucidate the reaction mechanism, we investigated several plausible scenarios (Figure 5). After Moore's hypothesis of photoionization and subsequent nucleophilic attack by the solvent (Figure 5C) was formulated,¹¹ another possible mechanism for photoinduced dehalogenation was reported by Fagnoni and co-workers for similar substrates.²⁸ This mechanism involves initial formation of an aryl cation by heterolytic cleavage of the C–Cl bond in the S₁ or T₁ state (Figure 5A).

Table 1. Reaction of 2 with Various Nucleophilic Solvents



Entry	Solvents	Product	NMR Yield (%)
1	H ₂ O	2-OH	a
2	MeOH	2-OMe	68
3	EtOH	2-OEt	60
4	<i>i</i> -PrOH	2-O- <i>i</i> -Pr	46
5	<i>t</i> -BuOH	2-O- <i>t</i> -Bu	20
6	MeCN	2-NHCOCH ₃	b

Reaction condition: A 0.002 M solution of **2** was irradiated at 350 nm for 2 hrs using a Rayonet reactor.
 a) Not able to determine the NMR yield as signals from the product and the starting material overlap.
 b) Only starting material was observed.

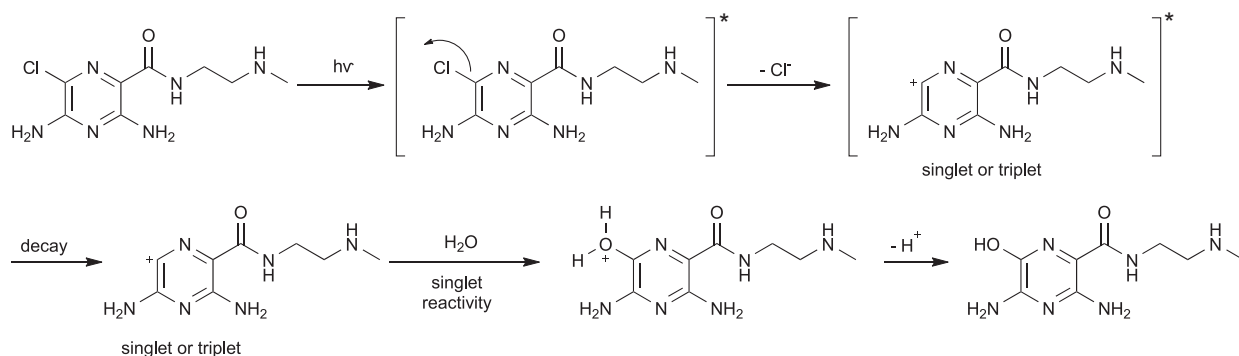
The resulting ground state singlet aryl cation then reacts with a nearby solvent molecule. We call this mechanism “photo-S_N1,” by analogy with its ground-state equivalent. We have further computationally investigated the possibility of a more traditional S_NAr mechanism in S₁ or T₁ (Figure 5B). For completeness, we also list photoreduction (Figure 5D), which is not observed for either 1² or 2 and which will not be considered further.

Photo-S_N1

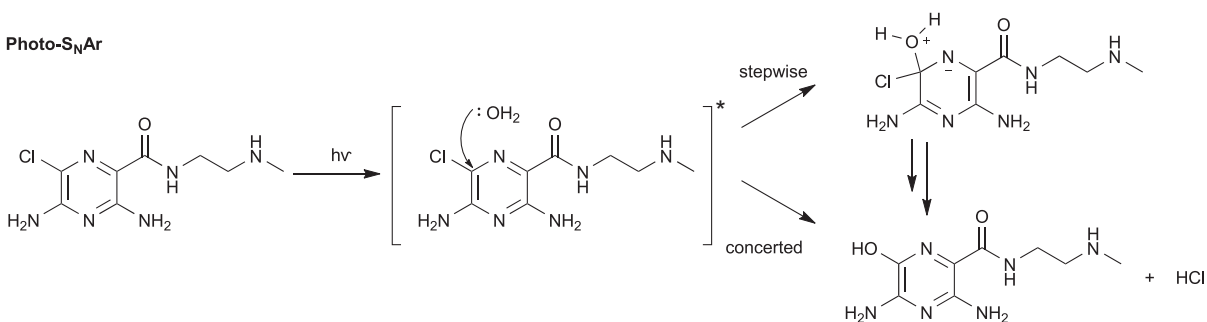
As an initial plausibility check of heterolytic chloride dissociation and aryl cation formation in S₁ and T₁, we used TD-DFT calculations on the model compound 2' (see Supplemental Information and Figure S1). The calculations showed a barrier for chloride dissociation of only 5.0 kcal/mol in the T₁ state and 5.4 kcal/mol in the S₁ state. These low barriers would make the reaction feasible at least in the T₁ state, given its longer lifetime. However, the calculations also showed that the reaction was endergonic both in T₁ (ΔG = 3.9 kcal/mol) and S₁ (ΔG = 5.0 kcal/mol), raising the question whether it would be disfavored thermodynamically. Given that dissociation would happen, the resulting aryl cation would relax to a ground state of either singlet or triplet multiplicity.²⁹ Our DFT calculations indicate that the triplet is the ground state, 1.6 kcal/mol below the singlet, which is also confirmed by high-level CASPT2 calculations (2.3 kcal/mol). The calculations show that the low-lying singlet aryl cation would add solvent molecules (H₂O, MeOH, *i*-PrOH, or *t*-BuOH) without any barrier, although the ground-state triplet cation is unreactive (see Supplemental Information and Figure S6). However, with an energy gap of only ~1 to 2 kcal/mol between singlet and triplet, inter-system crossing would be feasible and allow the triplet state to convert to the reactive singlet state. In summary, the photo-S_N1 mechanism seems plausible from a computational point of view, but as we shall see below, it turns out that it is not consistent with experimental findings.

To test the photo-S_N1 hypothesis experimentally, we turned to competition experiments. We first tested competition in solvent mixtures (Figure S30). The aryl cation

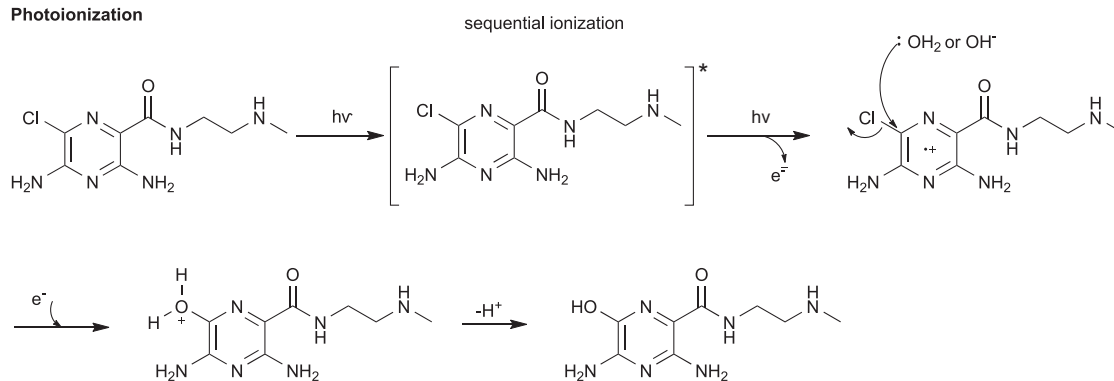
A Photo-S_N1



B Photo-S_NAr



C Photoionization



D Photoreduction

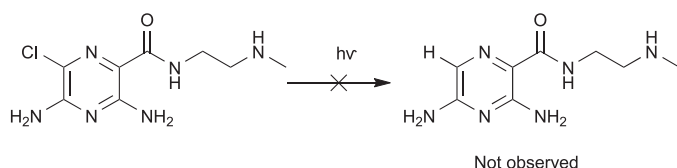
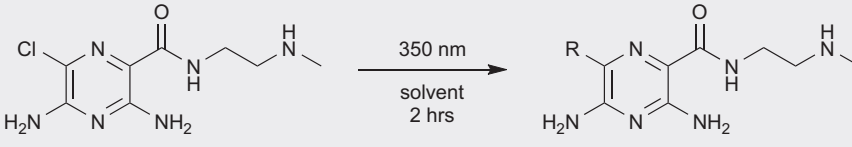


Figure 5. Investigated Mechanistic Scenarios

intermediate is extremely reactive and would not discriminate between nucleophiles. In MeOH/H₂O (1:1 v/v), 2-OH and 2-OMe were obtained in an equal ratio (Table 2, entry 1). As the molar ratio of MeOH to H₂O is 1:2.2, there is a slight preference for MeOH over H₂O as nucleophile. With MeOH/EtOH (1:1 v/v), a 3:1 mixture of 2-OMe and 2-OEt was obtained (Table 2, entry 2). As the molar ratio is only 1.4:1, MeOH is here preferred over EtOH. In MeOH/*i*-PrOH (1:1 v/v), eight times as much 2-OMe was obtained than 2-*O-i*-Pr, showing that MeOH is clearly superior to *i*-PrOH as nucleophile as the molar ratio is in its favor only by 1.9:1.

Table 2. Reaction of 2 in Solvent Mixtures



Entry	Solvent ratio (v/v)	Product	Product ratio	Solvent ratio
1	MeOH/H ₂ O (1:1)	2-OMe:2-OH	1:1	1:2.2
2	MeOH:EtOH (1:1)	2-OMe:2-OEt	3:1	1.4:1
3	MeOH: <i>i</i> -PrOH (1:1)	2-OMe: 2-O- <i>i</i> -Pr	8:1	1.9:1

Reaction condition: A 0.002 M solution of **2** was irradiated at 350 nm for 2 hrs using a Rayonet reactor.

See also [Figure S30](#).

Although the differences in reactivity between the different nucleophiles is strong evidence against the photo-S_N1 mechanism, they could in principle be consistent with subtle differences in preferential solvation of the aryl cation.³⁰ Therefore, we carried out another round of experiments. Aryl cations are known to coordinate to acetonitrile, resulting in the formation of acetamides after attack by water ([Figure 6](#)). This reaction, which is the photochemical equivalent of the Ritter reaction, has been observed previously for aryl cation intermediates of other compounds by Albini and co-workers.³¹ Our DFT calculations ([Supplemental Information](#); [Figure S2](#)) show that acetonitrile coordination to the singlet aryl cation of **2'** is highly exergonic ($\Delta G = -53.0$ kcal/mol). Subsequent addition of H₂O occurs with a barrier of 17.4 kcal/mol, which should be feasible at room temperature. Therefore, acetamide product **3** would be expected to form upon irradiating **2** in MeCN or MeCN/H₂O mixtures. However, irradiation in neat MeCN did not result in acetamide **3** or the alternative cyclized imidazopyrazine **4**. Irradiation in solvent mixtures of MeCN with MeOH or H₂O (9:1 v/v) only gave trace amounts of **2-OMe** and **2-OH**, respectively, and no evidence of **3** or **4**. If the aryl cation is formed, it should react statistically as addition of MeOH/H₂O and MeCN are all barrierless processes. Furthermore, irradiation of **2** at 365 nm in DMSO in the presence of KCN (10 equiv.) did not result in any cyano-substituted product. Also, no reaction occurred under irradiation in MeCN with tetrabutylammonium cyanide (TBACN) (10 equiv.).

Experiments with π nucleophiles also make the photo-S_N1 mechanism unlikely. The triplet aryl cation, which is predicted to be the ground state according to our calculations, should readily add π nucleophiles to give the allylated or vinylylated product, respectively.³¹ We tested reaction with both allyltrimethylsilane and styrene in MeCN/MeOH (9:1 v/v) with irradiation for 2 h at 365 nm, but no addition product was found ([Figure S31](#)). Lack of reactivity with styrene and allyltrimethylsilane also indicates that radicals are not generated during the reaction.

In conclusion, an array of experiments is inconsistent with the photo-S_N1 mechanism ([Figure 6](#)). The non-statistical outcomes of the competition experiments in mixed solvents and the lack of reactivity with MeCN and CN⁻ are not consistent with barrierless addition of the closest nucleophile to a very reactive singlet aryl cation intermediate. The lack of reactivity with π nucleophiles is not consistent with a triplet aryl cation intermediate. One possible explanation why the reaction does not occur

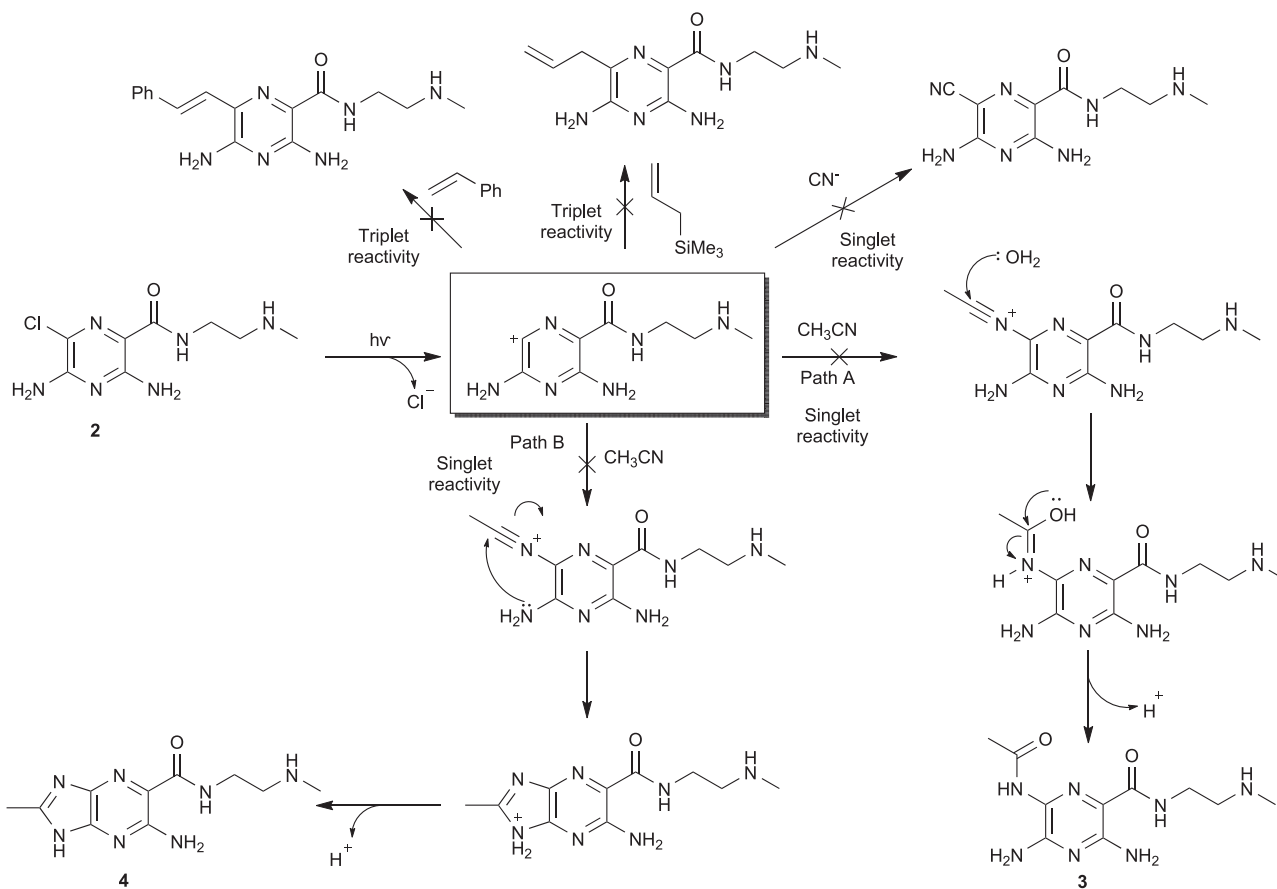


Figure 6. Experiments Excluding Aryl Cation Intermediate

Lack of triplet-state reactivity with styrene and allyltrimethylsilane and lack of singlet-state reactivity with CN^- and MeCN. Path A: proposed mechanisms of the photo-Ritter reaction in acetonitrile/water mixtures are shown. Path B: proposed reaction pathway for the formation of cyclized product imidazopyrazine **4** is shown.

despite the calculated small barrier is the endergonicity of the initial dissociation of Cl^- in S_1 and T_1 .

Concerted or Stepwise $\text{S}_{\text{N}}\text{Ar}$

We further considered the possibility that the photoreaction proceeds via a $\text{S}_{\text{N}}\text{Ar}$ mechanism in the excited state. However, DFT calculations showed a high barrier for attack by H_2O in the T_1 state (36.4 kcal/mol, using another H_2O as general base). This barrier is much too high for the reaction to take place in this short-lived excited state. Interestingly, the reaction is calculated to be concerted, with displacement of Cl^- occurring simultaneously with C–O bond formation. Considering OH^- as the nucleophile (standard state of 10^{-7} M) lowered the barrier to 18.9 kcal/mol, which we deem unlikely given the short lifetime of the excited state and that the reaction occurs even at low pH, where the concentration of OH^- is below 10^{-10} M (*vide infra*). The barrier is of similar magnitude in the S_1 $\pi\pi^*$ state (22.1 kcal/mol). For more details, see [Supplemental Information](#) and [Figure S3](#). Based on these calculations, the photo- $\text{S}_{\text{N}}\text{Ar}$ mechanism is highly implausible.

Photoionization

Having excluded the photo- $\text{S}_{\text{N}}1$ and photo- $\text{S}_{\text{N}}\text{Ar}$ mechanism, we then assessed photoionization followed by nucleophilic attack by the solvent ([Figure 5B](#)). As shown

previously in the context of photoredox catalysis, arene radical cations are much more prone to undergo S_NAr reactions than the neutral compounds.²² The photochemistry of **1** has previously been studied only in water. We investigated photoionization of **2** by photoelectrochemistry in MeOH, EtOH, and *i*-PrOH. A photocurrent corresponding to the release of solvated electrons was detected in MeOH and was found to correlate with light intensity and applied bias potential (see [Supplemental Experimental Procedures](#) and [Figure S17](#)). The formation of solvated electrons is in accordance with the flash photolysis experiments by Hamoudi.¹² Photocurrent measurements in a series of alcohols (MeOH, EtOH, and *i*-PrOH) detected similar photoinduced currents within experimental error in all tested solvents ([Figure S18](#)), in line with the observed formation of substitution products. The detection of a photocurrent for **2** in *i*-PrOH is different compared to **1**, for which Hamoudi detected solvated electrons in H₂O, but not in *i*-PrOH.

Hypothesizing that more electron-rich arenes should photoionize more efficiently, we compared the reactivity of **2** with its ester analog **S2** (see [Supplemental Experimental Procedures](#), [Supplemental Information](#), [Scheme S1](#), and [Figure S12](#)). Cyclic voltammetry showed that **S2** is more electron poor than **2**, as evidenced by its higher redox potential ([Figures S13–S16](#)). Consistent with its electronic properties, we observed smaller generated photocurrent and lower reactivity by a factor of 6 as compared to **2** ([Figure S34](#)). The monoamino-substituted pyrazine derivative **S1** has an even higher redox potential and no detectable photocurrent. Below, we discuss the influence of the frontier orbital energies for the rationalization of photoionization.

Although Hamoudi and co-workers argued that photoionization of **1** is a monophotonic process at 353 nm and a biphotonic process at 265 nm,¹² we find that this is not thermodynamically feasible. The calculated solution-phase vertical ionization potential ($I_{P_{\text{vert}}}$) of **2** is 6.08 eV (204 nm), very close to the 5.98 eV (207 nm) calculated for **1**. Considering the possibility of adiabatic ionization and that the electron is transferred to bulk water with a hydration enthalpy of -1.34 eV,³² the best-scenario cost of photoionization is reduced to 4.57 eV (271 nm) for **2** and 4.43 (280 nm) for **1**. Clearly, these values are still too high for a monophotonic process at 353 nm (3.51 eV), even allowing for a large error in the calculated values. As noted by Grabner and El-Gogary,³³ a linear relationship between laser power and concentration of solvated electrons, as was observed by Hamoudi, is not sufficient evidence to conclude a monophotonic process. Measurements over a wide range of irradiation powers and correcting for non-linear behavior with pulse energy would be needed, which was not done by Hamoudi.¹² For a more extensive discussion, see the [Supplemental Information](#) and [Table S2](#). We therefore conclude that the photoionization of **1** and **2**, as shown by the observed photo-current, is a biphotonic process not only at 265 nm but also at 353 nm. This sequential photoionization could progress either through the singlet or triplet excited states, although the triplet would be more likely considering its longer lifetime. Absorption of triplet **2** at 360 nm is supported by our TD-DFT calculations and comparison with experimental results for the amiloride triplet by Hamoudi et al. (see [Supplemental Information](#) and [Figure S48](#)).¹²

Having shown that photoionization occurs in all protic solvents investigated, we then turned to the next step of the reaction: nucleophilic attack on the radical cation. The nucleophile could be either a neutral or deprotonated solvent molecule, depending on the pH. DFT calculations showed that attack by H₂O on the model **2'**^{•+} occurs with a considerable barrier of 27.5 kcal/mol using the SMD implicit solvent model. However, the barrier was lowered considerably to 19.6 kcal/mol by adding another explicit water molecule acting as a general base. Barriers of similar height were

Table 3. Physical Properties of Alcoholic Solvents

	pK _{ap} ^a	pK _a ^b	N (RO ⁻) ^c
H ₂ O	14.0	15.7	10.47
MeOH	16.5–16.7	15.5	15.78
EtOH	18.7–19.5	15.9	15.78
<i>i</i> -PrOH	20.6–20.8	17.1	17.03
<i>t</i> -BuOH	28.5	19.2	–

Autoprotolysis constants, acid dissociation constants, and dielectric constants for the alcohols.

^aAutoprotolysis constants at 25°C.⁶⁹

^bAcid dissociations constants in water.⁷⁰

^cMayr nucleophilicity parameter for alkoxide in the corresponding alcohol.

obtained for 2^{•+} and were not affected significantly by protonation of the terminal amine (Supplemental Information; Figures S4 and S5). Considering the known limitations of DFT for reactions of charged species in solution, we believe that these barriers are consistent with reaction on the microsecond timescale, as dictated by the expected lifetime of the radical cation.^{34,35}

A competing pathway in neutral or slightly basic solution is attack by hydroxide or alkoxides. We measured the pH of a 0.8 mM aqueous solution of 2 to 8.5–8.7, which would mean a hydroxide concentration of ~4 μM (Supplemental Experimental Procedures). DFT calculations indicate that OH⁻ and MeO⁻ react with 2^{•+} in a barrierless manner, although EtO⁻, *i*-PrO⁻, and *t*-BuO⁻ show manageable barriers of 5.9 kcal/mol, 5.4 kcal/mol, and 11.1 kcal/mol, respectively (a standard state of 10⁻⁷ M is used for the alkoxides; see Supplemental Information and Figure S4). These computational results are consistent with the slower reactivity in EtOH, *i*-PrOH, and *t*-BuOH as compared to MeOH and H₂O (Table 1). However, there are also other plausible explanations for the observed difference in reactivity. One such explanation is the lower rates of autoprotolysis of the more substituted alcohols (Table 3). For example, the ambient concentration of OH⁻ in H₂O is 14 orders of magnitude larger than that of *t*-BuO⁻ in *t*-BuOH. As 2 is a weak base, the alcohols' pK_a is also relevant (Table 3). The more-substituted alcohols are harder to deprotonate, and we therefore expect lower concentrations of alkoxide nucleophile. The nucleophilicities of the alkoxide anions follow the same trend (Table 3).

To test the hypothesis that OH⁻ is the main active nucleophile, we performed competition experiments with AcO⁻ in a 1:1 ratio (v/v) of AcOH and H₂O. When both AcOH and H₂O are present, the ratio AcO⁻/OH⁻ should be determined by their relative pK_a, ~10¹². Detailed calculations show that AcO⁻ should be present in a concentration of ~0.02 M with a pH of 1.8, meaning that the ratio of AcO⁻ to OH⁻ is 3 × 10¹⁰ (see Supplemental Information). Computationally, we find that attack by AcO⁻ on 2^{•+} has a barrier of only 8.0 kcal/mol (10⁻² M standard state). In case the reactive species is the anion, acetate should therefore outcompete hydroxide by a wide margin. From the experiment performed in a 1:1 ratio (v/v) of AcOH and H₂O, we see trace amount of 2–OH by LC-MS (227 m/z) and no acetylated product 2–OAc. Although OH⁻ could well contribute at higher pH, we therefore find that H₂O must play a role and likely dominates the reactivity at neutral or low pH. As indicated by the calculations above, this reactivity would rely on general base catalysis to increase the nucleophilicity of H₂O. To test this hypothesis, we carried out irradiation of 2 in D₂O versus H₂O and found that the reaction in H₂O is ~10% faster than in D₂O (Figures S19, S20, and S32). This is clearly a solvent kinetic isotope effect (KIE), as expected if a selectivity-determining nucleophilic attack by a solvent

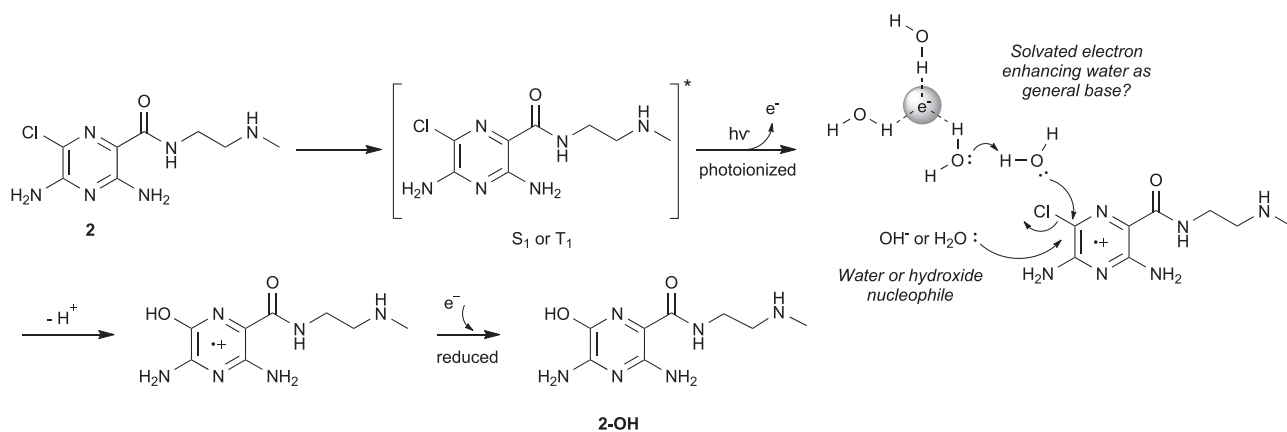


Figure 7. Suggested Mechanism for Photosubstitution of 2

Photoionization occurs by sequential absorption of two photons, with the second absorbed either from the S_1 state (less likely) or T_1 state (more likely). The resulting radical cation is attacked either by solvent or hydroxide/alkoxide with concerted loss of Cl^- . Deprotonation and recombination with the electron lead to the substitution product **2-OH**. The solvated electron plausibly acts as a general base to assist reactivity.

molecule is assisted by a general base. The observed rate enhancement is a function of a competition between the rate of nucleophilic attack and the unknown rate of electron recombination (leading back to starting material). We therefore cannot determine an exact value for the KIE, but we can see that it is clearly larger than one. We therefore conclude that the nucleophile at neutral and low pH must be the neutral species, assisted by a general base in solution. Another piece of evidence against OH^- as the active nucleophile comes from experiments by De Luca et al.¹⁴ They observed similar rates of formation of photoproduct at pH 3 and pH 7, even though the concentration of OH^- is negligible at pH 3 (10^{-11} M).

As the photochemical reaction is electroneutral, the radical cation must be reduced after the substitution step (Figure 7). This implies that the solvated electrons cannot quantitatively react with solvent to produce dihydrogen and hydroxide (alkoxide). Due to its negative charge, it may instead enhance the ability of the local water molecule to act as a general base toward the nucleophile in the substitution reaction, eventually recombining with the product radical cation to give the observed product. Considering that the solvent acts as nucleophile with a high effective concentration, we believe that this process is competitive with decay of the solvated electrons, which likely occurs on the microsecond timescale.³⁶

Excited-State Antiaromaticity as a Potential Driving Force for Photoionization

Having established that photoionization by sequential absorption of two photons is the most likely mechanism, we now turn to the question of driving force. One possible explanation for the facile photoionization of **2** is based on excited state antiaromaticity. Ground-state aromatic compounds become antiaromatic in their lowest singlet and triplet $\pi\pi^*$ states according to Baird's rule, the excited state equivalent of Hückel's rule.³⁷ Aromatic compounds are much more reactive when photoexcited,^{38,39} and it has recently been shown that new photochemical reactions can be developed with relief of excited state antiaromaticity as the driving force.^{40,41} We now hypothesize that excited state antiaromaticity can also be a driving force for photoionization from the excited state.

Aromaticity in the ground state is linked with high IPs,⁴² while non-aromatic and antiaromatic compounds display lower IPs (Figure 8A). The reason is that antiaromatic

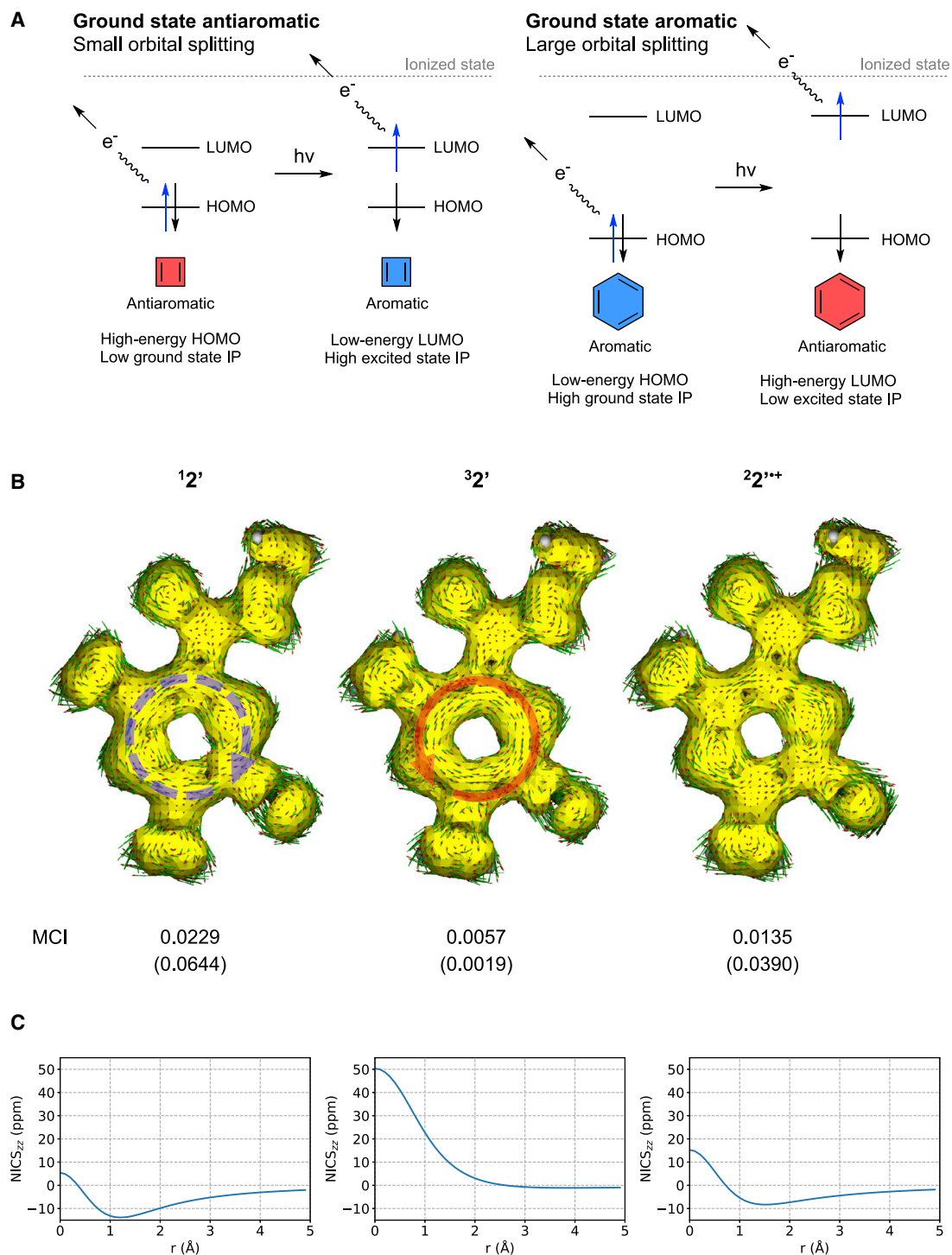


Figure 8. Aromaticity Analysis

(A) Qualitative explanation for why excited-state antiaromaticity leads to more facile sequential photoionization, as the LUMO level is relatively high for ground-state aromatic molecules.

(B) ACID plots of $2'$ show a moderate aromatic ring current in the S_0 state (left), antiaromatic ring current in the relaxed T_1 state (middle), and no aromatic ring current in the radical cation $2'^{+\bullet}$ (right). MCI values indicate moderate aromaticity for $2'$ in S_0 , very weak or no aromaticity for $2'^{+\bullet}$, and antiaromaticity for $2'$ in T_1 . Reference values for pyrazine are given in parenthesis.

(C) NICS scans show an aromatic minimum in S_0 for $2'$, shallow aromatic minimum for $2'^{+\bullet}$, and a clear antiaromatic maximum for the T_1 state. Calculations at the B3LYP/6-311+G(d,p) level are shown. ACID plots at 0.030 isosurface value are shown.

compounds have smaller frontier orbital splittings, and their HOMOs are consequently higher in energy than for aromatic compounds. Photoionization could occur either in a monophotonic process directly from the HOMO or from the LUMO in a biphotonic process via initial excitation to the excited state (HOMO \rightarrow LUMO). For the monophotonic process, ground state aromatic compounds like **2** should have a relatively high IP. For the biphotonic process, on the other hand, excitation occurs from a relatively high-lying LUMO and should be more facile. Within this context, removing an electron from the LUMO could be seen as a way for excited-state antiaromatic compounds to relieve their antiaromaticity. This qualitative picture is corroborated by our calculations, showing that the IPs decreases much more going from ground to excited state for ground-state aromatic compounds than for antiaromatic ones (see [Supplemental Information](#) and [Table S1](#)). Indeed, intramolecular charge transfer of an electron from an excited-state antiaromatic benzene ring was recently found to occur during photodissociation of a protecting group.^{43,44} Excited-state antiaromaticity is also involved in the fast excited-state deactivation of DNA base pairs, where it serves as a driving force for electron-driven proton transfer.⁴⁵

Now, how does the aromaticity of **2** change upon photoexcitation and subsequent ionization to the radical cation? We investigated this with calculations on the model compound **2'**. Ring currents according to the anisotropy of the induced current density (ACID) method⁴⁶ reveal a moderate diatropic (aromatic) ring current in the S_0 ground state of **2'**, while the relaxed T_1 state is antiaromatic with an appreciable paratropic ring current ([Figure 8B](#)). The aromaticity of **2'**, for which σ - π separation is possible, is further corroborated by the ACID plot based on only the π orbitals (see [Supplemental Information](#) and [Figure S47](#)). Photoionization to the radical cation **2'•+** is accompanied by loss of antiaromaticity, leading to non-aromaticity. These findings are further corroborated by multicenter index (MCI) calculations ([Figure 8B](#)) and nucleus-independent chemical shift (NICS) scans ([Figure 8C](#)).^{47–49} Furthermore, the similar MCI values for the relaxed T_1 (0.0057) and S_1 states (0.0089) indicate that the S_1 state of **2'** is also antiaromatic. The loss of aromaticity according to MCI is consistent with that for the parent pyrazine going from the ground state (0.0644) to the corresponding $\pi\pi^*$ triplet (0.0019) and singlet (0.0061) excited states. Due to the longer T_1 than S_1 lifetime, it is likely that photoexcitation occurs from the T_1 state. In summary, a contributing factor to the facile photoionization of **2** could therefore be antiaromaticity in the excited state, which is alleviated when going from the T_1 state to the radical cation.

We have studied the apparent photo- S_NAr reaction of amiloride analogs by a combination of experimental and theoretical methods to evaluate possible reaction mechanisms. The simplest possibility, a conventional S_NAr reaction in the excited state, can be excluded by the high calculated barriers in both singlet and triplet states. It is therefore clear that the excited state needs to evolve to a more reactive state. This could occur by dissociation of the chloride in an S_N1 -type fashion, giving an aryl cation, or by ionization, giving an arene radical cation. Heterolytic chloride dissociation is found to be possible, albeit endergonic. However, the observed reactivity profile does not agree with either a singlet or triplet aryl cation, and we can therefore exclude a photo- S_N1 reaction pathway. Due to the antiaromaticity of the excited state, the energy of the excited electron is high, but not sufficiently high for spontaneous ionization. However, a second photon can eject the electron into the surrounding solvent. The solvated electrons are detected, giving support for the ionization hypothesis. The experimental selectivity profile combined with calculated barriers indicates that the radical cation reacts with a neutral solvent molecule,

assisted by another solvent molecule acting as a general base. It is plausible that the basicity of the solvent is strengthened by the nearby solvated electron. We have observed that several protic solvents are competent nucleophiles, but neutral solvents, such as acetonitrile, are unreactive, giving further support to the hypothesis that a general base is necessary for reactivity.

From a pharmaceutical perspective, understanding the degradation mechanism is the first step in creating predictive tools able to alert developers of drugs to potential light sensitivity. The mechanism studied here could also be an important tool to understand the fate of agrochemicals, which generally are exposed to light, water, and air in the environment. In organic synthesis, the reaction studied here is closely related to recent advances allowing mild S_NAr reactions of electron-rich substrates.²²

EXPERIMENTAL PROCEDURES

Resource Availability

Lead Contact

Further information and requests should be directed to the lead contact, Per-Ola Norrby (per-ola.norrby@astrazeneca.com).

Materials Availability

This study did not generate new unique reagents.

Data and Code Availability

Cartesian coordinates for all the computed structures can be found in the separately provided [Data S1](#) file.

Synthesis

Synthesis of 3,5-diamino-6-chloro-*N*-(2-(methylamino)ethyl)pyrazine-2-carboxamide (**2**) was carried out as reported in the literature ([Figure 4](#)).²⁹ To the methyl 3,5-diamino-6-chloropyrazine-2-carboxylate **S2** (4.94 mmol), the 2-(methylamino)ethylamine (24.68 mmol) was added and heated neat for 18 h at 120°C in a microwave sealed tube. The residual amine was removed under reduced pressure and diluted with acetonitrile. The precipitate formed was filtered and washed with acetonitrile to furnish a brown solid in 60% isolated yield. Characterization of the products and photoproducts in terms of NMR and LC-MS are given in [Figures S21–S28](#), [S33](#), and [S35–S39](#).

Spectroscopy

Absorption spectra were obtained on a scanning UV visible (UV-vis) spectrometer and a diode-array UV-vis spectrometer with matched 1.0-cm quartz cells. Fluorescence spectra were recorded on a diode-array automated combined luminescence and UV-vis spectrometer in 1.0-cm quartz fluorescence cuvettes at 23°C ± 1°C. The sample concentration was set to keep the absorbance below 0.5 at λ_{irr} , and a correction for self-absorption was applied for each spectrum. Emission spectra were also corrected using standard correction files. Each sample was measured 3–5 times, and the spectra were averaged. Due to the photosensitivity of the compounds, fresh samples were used for each measurement.

Cyclic Voltammetry

The electrochemistry was recorded in methanolic solutions of pyrazine derivative ($c = 1$ mM) using tetrabutylammonium hexafluorophosphate as a conducting salt ($c = 0.1$ M). The electrochemical measurements were accomplished using a

glassy-carbon disc working electrode, a platinum counter electrode, and a silver pseudo-reference electrode. The cyclic voltammograms in the measurement range (+1.2 V to -0.7 V) were recorded three times.

Standard Photochemical Experimental Procedure

The photochemical reactions were carried out for 2 h in a Rayonet reactor with 16 UV lamps (300–460 nm; $\lambda_{\text{max}} = 350$ nm). Solutions of concentration 2 mM in quartz test tubes were degassed by bubbling with argon for 10 min prior to irradiation. After 2 h of irradiation, residual solvent was removed under reduced pressure and the crude product was analyzed using ^1H NMR and LC-MS.

Experiments with π Nucleophiles

Allyltrimethylsilane and styrene (30 equiv.) were added to two independent quartz test tubes containing **2** in MeCN/MeOH (9:1, v/v). The test tubes were sealed with rubber septa, degassed using argon for 10 min, and irradiated for 2 h at 350 nm. Excess solvent was removed under reduced pressure, and the crude products were analyzed using ^1H NMR. In both the cases, only traces of **2-OMe** were observed and no addition product could be seen. Most of the starting material remained unreactive. Allyltrimethylsilane was completely consumed after irradiation, as shown by ^1H NMR (Supplemental Information; Figure S31). The allyltrimethylsilane was probably consumed by protodesilylation under the slightly acidic conditions to give volatile propene.⁵⁰ Importantly, neither styrene nor allyltrimethylsilane show any absorbance above 300 nm (Figure S11) and were therefore not photoexcited.

Solvent Isotopic Experiments

Two separate 2 mM solutions of compound **2** were prepared in H_2O and D_2O . The solutions were then degassed for ~ 20 min by bubbling with argon and irradiated simultaneously in the Rayonet reactor with 18 350-nm UV lamps. After every 30 min of irradiation, samples were carefully withdrawn from the solutions while maintaining the inert atmosphere in the reaction flask using argon. The residual solvent was removed under reduced pressure, and the crude ^1H NMR spectra were recorded and analyzed for NMR yield. The solutions were irradiated for a total period of 2 h.

Photocurrent Experiments

The photocurrent measurements were accomplished using a spectroelectrochemical cell irradiated with a UV light source. The light was gradually turned on and off, and the induced photocurrent was measured by a chronoamperometric method, applying a bias potential to accelerate the ionized electrons toward the electrode. A detailed description of experimental procedure is shown in the Supplemental Experimental Procedures. See Table S4 and Figures S40–S46 for absorption and emission characteristics of the studied amiloride derivatives.

Quantum-Chemical Calculations

All quantum-chemical calculations, unless otherwise noted, were carried out with Gaussian 16, revisions A.03 and B.01.⁵¹ Geometry optimizations were done at the B3LYP-D3(BJ)/6-31+G(d)/SMD level, i.e., with the B3LYP functional,⁵² the 6-31+G(d) basis set,⁵³ the SMD solvation model,⁵⁴ and the D3-BJ dispersion model.⁵⁵ Stationary points on the potential energy surface were confirmed with frequency calculations and transition states corroborated by quick reaction coordinate calculations.⁵⁶ Final energies were obtained from M06-2X-D3/6-311+G(d,p)/SMD single point calculations at the B3LYP geometries, i.e., using the M06-2X functional,⁵⁷

the 6-311+G(d,p) basis set,⁵⁸ the SMD solvent model, and the D3 dispersion model,⁵⁹ together with thermal contributions from B3LYP-D3(BJ)/6-31+G(d)/SMD. Standard-state corrections were applied to give a standard state of 1 M for reactants and 55.5 M for H₂O, unless otherwise noted. Triplet-state calculations used the same levels of theory but with unrestricted DFT.

Optimization and frequency calculations in the excited S₁ state used TD-DFT with B3LYP-D3(BJ)/6-31+G(d)/SMD based on a ground-state restricted reference. Final energies were obtained by combining the thermal corrections at the optimization level of theory with single-point energies at the M06-2X/6-311+G(d,p)/SMD level, enforcing equilibrium solvation treatment with the keyword "IOp(9/73=2)." MS-CASPT2^{60,61} calculations of the aryl cations were done with OpenMolcas 18.0⁶² with an active space of 6 electrons in 7 orbitals and the ANO-RCC-VDZP basis set.⁶³ An imaginary shift of 0.2 a.u. and an IPEA shift of 0.0 a.u.⁶⁴ were used. Further details on the reference wave function and active space orbitals can be found in the [Supplemental Experimental Procedures](#) and [Figures S7–S9](#).

Ionization potentials and electron affinities were calculated with the Δ SCF approach, using the energy of the neutral molecule and its radical anion/cation. Vertical values were obtained by single-point calculations of the anion/cation at the geometry of the parent molecule, although adiabatic values were obtained by allowing the anion/cation to relax. For vertical values, we used the electronic energy difference, and for adiabatic values, we used the free-energy difference.

NICS scans^{52,53} were performed with Aroma 1.0⁶⁵ and ACID plots⁴⁶ with the AICD 2.0.0 package, both using Gaussian 09, revision E.01.⁶⁶ MCI values⁵⁴ were obtained using the ESI-3D program,⁶⁷ based on the Quantum Theory of Atoms in Molecules atomic partition and the integration scheme as provided by the AIMAll package.⁶⁸ MCI values for pyrazine in the lowest $\pi\pi^*$ triplet state and its radical cation were calculated by optimizing the structures in D_{2h} symmetry with the orbital occupation altered (keyword "guess=alter") and employing symmetry in the SCF calculation (keyword "scf=symm"). For the $\pi\pi^*$ singlet excited state, we used TD-DFT, optimizing the third root. For the singlet and triplet states, the D_{2h} -symmetric geometry was not a minimum.

SUPPLEMENTAL INFORMATION

Supplemental Information can be found online at <https://doi.org/10.1016/j.xcrp.2020.100274>.

ACKNOWLEDGMENTS

The Olle Engkvist Byggmästare Foundation is greatly acknowledged for postdoctoral fellowships to T.S. and W.R. (184-390 and 194-677). T.S. appreciates support from the Institute of Organic Chemistry and Biochemistry of the Czech Academy of Sciences and the Czech Science Foundation (19-20467Y). H.O., K.J., and N.P.V. are grateful to the Swedish Research Council (VR) for financial support (2015-04538 and 2019-05618) and to the VINNOVA agency for an academia-industry exchange grant (2016-04572). K.J. is a fellow of the AstraZeneca post doc program. The computations were enabled by resources provided by the Swedish National Infrastructure for Computing (SNIC) at the Tetralith supercomputer at the National Supercomputer Centre in Sweden (NSC) at Linköping University, partially funded by the Swedish Research Council through grant agreement no. 2016-07213. We

are grateful to Joakim Bergman for assistance in initial photodegradation experiments.

AUTHOR CONTRIBUTIONS

K.J. carried out the majority of the computational work and co-wrote the manuscript. W.R. contributed the synthesis and carried out the bulk of the experiments and co-wrote the manuscript. T.S. carried out the photoelectrochemical and spectroscopic characterization and co-wrote the manuscript. N.P.V. carried out the MCI and some of the ionization potential calculations and co-wrote the manuscript. S.S. and J.W.L. carried out preliminary experiments. P.-O.N. and H.O. conceived the project, led the work, and co-wrote the manuscript.

DECLARATION OF INTERESTS

The authors declare no competing interests.

Received: September 9, 2020

Revised: October 30, 2020

Accepted: November 4, 2020

Published: December 16, 2020

REFERENCES

- Andersson, T., Broo, A., and Evertsson, E. (2014). Prediction of drug candidates' sensitivity toward autoxidation: computational estimation of C-H dissociation energies of carbon-centered radicals. *J. Pharm. Sci.* *103*, 1949–1955.
- Tonnesen, H.H. (2004). *Photostability of Drugs and Drug Formulations, Second Edition* (CRC).
- Trautwein, C., and Kümmerer, K. (2012). Degradation of the tricyclic antipsychotic drug chlorpromazine under environmental conditions, identification of its main aquatic biotic and abiotic transformation products by LC-MSⁿ and their effects on environmental bacteria. *J. Chromatogr. B Analyt. Technol. Biomed. Life Sci.* *889-890*, 24–38.
- Kochevar, K.E. (1981). Phototoxicity mechanisms: chlorpromazine photosensitized damage to DNA and cell membranes. *J. Invest. Dermatol.* *77*, 59–64.
- García, C., Piñero, L., Oyola, R., and Arce, R. (2009). Photodegradation of 2-chloro substituted phenothiazines in alcohols. *Photochem. Photobiol.* *85*, 160–170.
- Moore, D.E., Roberts-Thomson, S., Zhen, D., and Duke, C.C. (1990). Photochemical studies on the anti-inflammatory drug diclofenac. *Photochem. Photobiol.* *52*, 685–690.
- Moore, D.E., and Sithipitaks, V. (1983). Photolytic degradation of frusemide. *J. Pharm. Pharmacol.* *35*, 489–493.
- Moore, D.E., and Hemmens, V.J. (1982). Photosensitization by antimalarial drugs. *Photochem. Photobiol.* *36*, 71–77.
- Tamat, S.R., and Moore, D.E. (1983). Photolytic decomposition of hydrochlorothiazide. *J. Pharm. Sci.* *72*, 180–183.
- Moore, D.E. (1998). Photochemistry of diuretic drugs in solution. In *Drugs: Photochemistry and Photostability Special Publications*, A. Albini and E. Fasani, eds. (The Royal Society of Chemistry), pp. 100–115.
- Li, Y.N.B., Moore, D.E., and Tattam, B.N. (1999). Photodegradation of amiloride in aqueous solution. *Int. J. Pharm.* *183*, 109–116.
- Hamoudi, H.I., Heelis, P.F., Jones, R.A., Navaratnam, S., Parsons, B.J., Phillips, G.O., Vandenburg, M.J., and Currie, W.J.C. (1984). A laser flash photolysis and pulse radiolysis study of amiloride in aqueous and alcoholic solution. *Photochem. Photobiol.* *40*, 35–39.
- Calza, P., Massolino, C., Monaco, G., Medana, C., and Baiocchi, C. (2008). Study of the photolytic and photocatalytic transformation of amiloride in water. *J. Pharm. Biomed. Anal.* *48*, 315–320.
- De Luca, M., Ioele, G., Mas, S., Tauler, R., and Ragno, G. (2012). A study of pH-dependent photodegradation of amiloride by a multivariate curve resolution approach to combined kinetic and acid-base titration UV data. *Analyst (Lond.)* *137*, 5428–5435.
- Leng, T.-D., Si, H.-F., Li, J., Yang, T., Zhu, M., Wang, B., Simon, R.P., and Xiong, Z.-G. (2016). Amiloride analogs as ASIC1a inhibitors. *CNS Neurosci. Ther.* *22*, 468–476.
- Liu, W., Li, J., Huang, C.-Y., and Li, C.-J. (2020). Aromatic chemistry in the excited state: facilitating metal-free substitutions and cross-couplings. *Angew. Chem. Int. Ed. Engl.* *59*, 1786–1796.
- Rossi, R.A., Pierini, A.B., and Peñeñory, A.B. (2003). Nucleophilic substitution reactions by electron transfer. *Chem. Rev.* *103*, 71–167.
- Pandey, G., Krishna, A., and Rao, J.M. (1986). Single electron transfer initiated photocyclization of substituted cinnamic acids to corresponding coumarins. *Tetrahedron Lett.* *27*, 4075–4076.
- Fukuzumi, S., and Ohkubo, K. (2014). Organic synthetic transformations using organic dyes as photoredox catalysts. *Org. Biomol. Chem.* *12*, 6059–6071.
- Das, S., Natarajan, P., and König, B. (2017). Teaching old compounds new tricks: DDQ-photocatalyzed C-H amination of arenes with carbamates, urea, and N-heterocycles. *Chemistry* *23*, 18161–18165.
- Zheng, Y.-W., Chen, B., Ye, P., Feng, K., Wang, W., Meng, Q.-Y., Wu, L.-Z., and Tung, C.-H. (2016). Photocatalytic hydrogen-evolution cross-couplings: benzene C-H amination and hydroxylation. *J. Am. Chem. Soc.* *138*, 10080–10083.
- Romero, N.A., Margrey, K.A., Tay, N.E., and Nicewicz, D.A. (2015). Site-selective arene C-H amination via photoredox catalysis. *Science* *349*, 1326–1330.
- Glaser, F., Kerzig, C., and Wenger, O.S. (2020). Multi-photon excitation in photoredox catalysis: concepts, applications, methods. *Angew. Chem. Int. Ed. Engl.* *59*, 10266–10284.
- Ghosh, I., Ghosh, T., Bardagi, J.I., and König, B. (2014). Reduction of aryl halides by consecutive visible light-induced electron transfer processes. *Science* *346*, 725–728.
- Giedyk, M., Narobe, R., Weiß, S., Touraud, D., Kunz, W., and König, B. (2020). Photocatalytic activation of alkyl chlorides by assembly-promoted single electron transfer in microheterogeneous solutions. *Nat. Catal.* *3*, 40–47.
- Hunt, T., Atherton-Watson, H.C., Axford, J., Collingwood, S.P., Coote, K.J., Cox, B., Czarnecki, S., Danahay, H., Devereux, N., Howsham, C., et al. (2012). Discovery of a novel

- chemotype of potent human ENaC blockers using a bioisostere approach. Part 1: quaternary amines. *Bioorg. Med. Chem. Lett.* **22**, 929–932.
27. Mazzo, D.J. (1986). Amiloride hydrochloride. In *Analytical Profiles of Drug Substances*, K. Florey, ed. (Academic), pp. 1–34.
 28. Dichiarante, V., Protti, S., and Fagnoni, M. (2017). Phenyl cation: a versatile intermediate. *J. Photochem. Photobiol. Chem.* **339**, 103–113.
 29. Lazzaroni, S., Dondi, D., Fagnoni, M., and Albini, A. (2008). Geometry and energy of substituted phenyl cations. *J. Org. Chem.* **73**, 206–211.
 30. Reichardt, C. (2003). *Solvents and Solvent Effects in Organic Chemistry*, Third Edition (Wiley-VCH).
 31. Protti, S., Dichiarante, V., Dondi, D., Fagnoni, M., and Albini, A. (2012). Singlet/triplet phenylcations and benzyne from the photodehalogenation of some silylated and stannylated phenyl halides. *Chem. Sci.* **3**, 1330–1337.
 32. Donald, W.A., Demireva, M., Leib, R.D., Aiken, M.J., and Williams, E.R. (2010). Electron hydration and ion-electron pairs in water clusters containing trivalent metal ions. *J. Am. Chem. Soc.* **132**, 4633–4640.
 33. El-Gogary, S., and Grabner, G. (2006). Ultraviolet photoionization of the photosensitizers khellin and visnagin in aqueous solution and in micelles: one-photon ionization is a minor process. *Photochem. Photobiol. Sci.* **5**, 311–316.
 34. Pan, J.-X., Han, Z.-H., Miao, J.-L., Yao, S.-D., Lin, N.-Y., and Zhu, D.-Y. (2001). Furanochromone radical cations: generation, characterization and interaction with DNA. *Biophys. Chem.* **91**, 105–113.
 35. Selvaraju, C., and Ramamurthy, P. (2004). Excited-state behavior and photoionization of 1,8-acridinedione dyes in micelles—comparison with NADH oxidation. *Chemistry* **10**, 2253–2262.
 36. Taub, I.A., Harter, D.A., Sauer, M.C., and Dorfman, L.M. (1964). Pulse radiolysis studies. IV. The solvated electron in the aliphatic alcohols. *J. Chem. Phys.* **41**, 979–985.
 37. Baird, N.C. (1972). Quantum organic photochemistry. II. Resonance and aromaticity in the lowest ${}^3\pi\pi^*$ state of cyclic hydrocarbons. *J. Am. Chem. Soc.* **94**, 4941–4948.
 38. Rosenberg, M., Dahlstrand, C., Kilså, K., and Ottosson, H. (2014). Excited state aromaticity and antiaromaticity: opportunities for photophysical and photochemical rationalizations. *Chem. Rev.* **114**, 5379–5425.
 39. Papadakis, R., and Ottosson, H. (2015). The excited state antiaromatic benzene ring: a molecular Mr Hyde? *Chem. Soc. Rev.* **44**, 6472–6493.
 40. Mohamed, R.K., Mondal, S., Jorner, K., Delgado, T.F., Lobodin, V.V., Ottosson, H., and Alabugin, I.V. (2015). The missing C1-C5 cycloaromatization reaction: triplet state antiaromaticity relief and self-terminating photorelease of formaldehyde for synthesis of fulvenes from enynes. *J. Am. Chem. Soc.* **137**, 15441–15450.
 41. Papadakis, R., Li, H., Bergman, J., Lundstedt, A., Jorner, K., Ayub, R., Halder, S., Jahn, B.O., Denisova, A., Zietz, B., et al. (2016). Metal-free photochemical silylations and transfer hydrogenations of benzenoid hydrocarbons and graphene. *Nat. Commun.* **7**, 12962.
 42. Gershoni-Poranne, R., Rahalkar, A.P., and Stanger, A. (2018). The predictive power of aromaticity: quantitative correlation between aromaticity and ionization potentials and HOMO-LUMO gaps in oligomers of benzene, pyrrole, furan, and thiophene. *Phys. Chem. Chem. Phys.* **20**, 14808–14817.
 43. Halder, D., and Paul, A. (2020). Understanding the role of aromaticity and conformational changes in bond dissociation processes of photo-protecting groups. *J. Phys. Chem. A* **124**, 3976–3983.
 44. Banerjee, A., Halder, D., Ganguly, G., and Paul, A. (2016). Deciphering the cryptic role of a catalytic electron in a photochemical bond dissociation using excited state aromaticity markers. *Phys. Chem. Chem. Phys.* **18**, 25308–25314.
 45. Karas, L.J., Wu, C.-H., Ottosson, H., and Wu, J.I. (2020). Electron-driven proton transfer relieves excited-state antiaromaticity in photoexcited DNA base pairs. *Chem. Sci.* **11**, 10071–10077.
 46. Geuenich, D., Hess, K., Köhler, F., and Herges, R. (2005). Anisotropy of the induced current density (ACID), a general method to quantify and visualize electronic delocalization. *Chem. Rev.* **105**, 3758–3772.
 47. Stanger, A. (2006). Nucleus-independent chemical shifts (NICS): distance dependence and revised criteria for aromaticity and antiaromaticity. *J. Org. Chem.* **71**, 883–893.
 48. Jiménez-Halla, J.O.C., Matito, E., Robles, J., and Solà, M. (2006). Nucleus-independent chemical shift (NICS) profiles in a series of monocyclic planar inorganic compounds. *J. Organomet. Chem.* **691**, 4359–4366.
 49. Bultinck, P., Ponec, R., and Van Damme, S. (2005). Multicenter bond indices as a new measure of aromaticity in polycyclic aromatic hydrocarbons. *J. Phys. Org. Chem.* **18**, 706–718.
 50. Hosomi, A., and Sakurai, H. (1976). Syntheses of γ,δ -unsaturated alcohols from allylsilanes and carbonyl compounds in the presence of titanium tetrachloride. *Tetrahedron Lett.* **17**, 1295–1298.
 51. Frisch, M.J., Trucks, G.W., Schlegel, H.B., Scuseria, G.E., Robb, M.A., Cheeseman, J.R., Scalmani, G., Barone, V., Petersson, G.A., Nakatsuji, H., et al. (2016). Gaussian 16, revision A.03 and B.01 (Gaussian).
 52. Stephens, P.J., Devlin, F.J., Chabalowski, C.F., and Frisch, M.J. (1994). Ab initio calculation of vibrational absorption and circular dichroism spectra using density functional force fields. *J. Phys. Chem.* **98**, 11623–11627.
 53. Ditchfield, R., Hehre, W.J., and Pople, J.A. (1971). Self-consistent molecular-orbital methods. IX. An extended gaussian-type basis for molecular-orbital studies of organic molecules. *J. Chem. Phys.* **54**, 724–728.
 54. Marenich, A.V., Cramer, C.J., and Truhlar, D.G. (2009). Universal solvation model based on solute electron density and on a continuum model of the solvent defined by the bulk dielectric constant and atomic surface tensions. *J. Phys. Chem. B* **113**, 6378–6396.
 55. Grimme, S., Ehrlich, S., and Goerigk, L. (2011). Effect of the damping function in dispersion corrected density functional theory. *J. Comput. Chem.* **32**, 1456–1465.
 56. Goodman, J.M., and Silva, M.A. (2003). QRC: a rapid method for connecting transition structures to reactants in the computational analysis of organic reactivity. *Tetrahedron Lett.* **44**, 8233–8236.
 57. Zhao, Y., and Truhlar, D.G. (2008). The M06 suite of density functionals for main group thermochemistry, thermochemical kinetics, noncovalent interactions, excited states, and transition elements: two new functionals and systematic testing of four M06-class functionals and 12 other functionals. *Theor. Chem. Acc.* **120**, 215–241.
 58. Krishnan, R., Binkley, J.S., Seeger, R., and Pople, J.A. (1980). Self-consistent molecular orbital methods. XX. A basis set for correlated wave functions. *J. Chem. Phys.* **72**, 650–654.
 59. Grimme, S., Antony, J., Ehrlich, S., and Krieg, H. (2010). A consistent and accurate ab initio parametrization of density functional dispersion correction (DFT-D) for the 94 elements H-Pu. *J. Chem. Phys.* **132**, 154104.
 60. Finley, J., Malmqvist, P.-Å., Roos, B.O., and Serrano-Andrés, L. (1998). The multi-state CASPT2 method. *Chem. Phys. Lett.* **288**, 299–306.
 61. Andersson, K., Malmqvist, P.-Å., and Roos, B.O. (1992). Second-order perturbation theory with a complete active space self-consistent field reference function. *J. Chem. Phys.* **96**, 1218–1226.
 62. Aquilante, F., Autschbach, J., Carlson, R.K., Chibotaru, L.F., Delcey, M.G., De Vico, L., Fdez Galván, I., Ferré, N., Frutos, L.M., Gagliardi, L., et al. (2016). Molcas 8: new capabilities for multiconfigurational quantum chemical calculations across the periodic table. *J. Comput. Chem.* **37**, 506–541.
 63. Roos, B.O., Lindh, R., Malmqvist, P.-Å., Veryazov, V., and Widmark, P.-O. (2004). Main group atoms and dimers studied with a new relativistic ANO basis set. *J. Phys. Chem. A* **108**, 2851–2858.
 64. Zobel, J.P., Nogueira, J.J., and González, L. (2017). The IPEA dilemma in CASPT2. *Chem. Sci. (Camb.)* **8**, 1482–1499.
 65. Technion - Israel Institute of Technology (2020). Amnon Stranger. <http://chemistry.technion.ac.il/members/amnon-stanger/>.
 66. Frisch, M.J., Trucks, G.W., Schlegel, H.B., Scuseria, G.E., Robb, M.A., Cheeseman, J.R., Scalmani, G., Barone, V., Mennucci, B.,

- Peterson, G.A., et al. (2016). Gaussian 09, revision E.01 (Gaussian).
67. Matito, E. (2006). ESI-3D: electron sharing indices program for 3D molecular space partitioning. <http://iqcc.udg.edu/~eduard/ESI/>.
68. TK Gristmill Software (2018). AIMAll (Version 17.11.14 B). <http://aim.tkgristmill.com>.
69. Rondinini, S., Longhi, P., Mussini, P.R., and Mussini, T. (1987). Autoprotolysis constants in nonaqueous solvents and aqueous organic solvent mixtures. *Pure Appl. Chem.* 59, 1693–1702.
70. Anslyn, E.V., and Dougherty, D.A. (2005). *Modern Physical Organic Chemistry* (University Science).